The Complex Role of Storms in Modulating Air-Sea CO_2 Fluxes in the sub-Antarctic Southern Ocean.

Tesha Toolsee[1,2,*], Sarah-Anne Nicholson[1], Pedro M.S. Monteiro[3]

[1] Southern Ocean Carbon-Climate Observatory (SOCCO), CSIR, Cape Town, South Africa

[2] Department of Oceanography, University of Cape Town, Cape Town, South Africa

[3] School for Climate Studies, Stellenbosch University, Stellenbosch, South Africa

*Corresponding author: Tesha Toolsee (TLSTES001@myuct.ac.za)

Key Points:

- Hourly glider observations show that the impact of storms on both k_w and ΔpCO_2 simultaneously modulates the magnitude of FCO_2 variability.
- Winter-spring storms weaken ΔpCO_2 through enhanced entrainment and mixing, counteracting the expected increase in FCO_2 due to k_w alone.
- By not accounting for the storm feedback in both k_w and ΔpCO_2, the magnitude of the FCO_2 was found to be overestimated (by 6.6 - 26.5%).

Abstract

The intra-seasonal CO_2 flux (FCO_2) variability across the Southern Ocean is poorly understood due to sparse observations at the required temporal and spatial scales. Twinned Waveglider-Seaglider experiments were used to investigate how storms influence FCO_2 through both the gas transfer velocity (k_w) and the air-sea gradient in partial pressure of CO_2 (ΔpCO_2) in the sub-Antarctic zone. Winter-spring storms caused ΔpCO_2 to weaken (by 15-55 µatm) due to mixing/entrainment and weaker stratification. This response in ΔpCO_2 was in phase with k_w resulting in a counteractive weakening in FCO_2 (by 6.6 - 26.5% per storm), despite the wind-driven increase in k_w. Stronger stratification during summer explained the weaker sensitivity of ΔpCO_2 to storms, instead its thermal drivers dominated the ΔpCO_2 variability. These results highlight the importance of observing synoptic-scale variability in ΔpCO_2, the absence of which may propagate

significant biases to the mean annual FCO_2 estimates from large-scale observing programmes and reconstructions.

Plain Language Summary

The sub-Antarctic zone of the Southern Ocean is a region that mostly experiences carbon dioxide (CO_2) uptake because of its low temperature and strong winds. The wind can influence the CO_2 uptake through two pathways: the speed of CO_2 transfer between the air-sea interface (k_w) and the difference in CO_2 concentration in the surface ocean and overlying atmosphere (ΔpCO_2). Using autonomous robots that can measure hourly air and water conditions simultaneously, we show that not resolving ΔpCO_2 during a storm event can lead to overestimating the CO_2 uptake. This is particularly important during winter and spring when the ocean's surface layers are less stratified. The warmer temperatures during summer meant a more stratified surface layer resulting in a weaker and delayed impact of storms on the ΔpCO_2. This study shows that the various annual CO_2 uptake estimation methods used by the research community should not neglect ΔpCO_2 responses during storms.

1. Introduction

The sub-Antarctic zone (SAZ) of the Southern Ocean (SO) is a critical region in the global carbon cycle due to its ability to uptake (~1 Pg C yr^{-1}) large amounts of anthropogenic CO_2 (Figure 1a; DeVries et al., 2017; Gruber et al., 2019). Extra-tropical cyclones (hereafter referred to as storms) are prevalent synoptic features in the SO that occur at a 4 to 8-day frequency (Yuan, 2004; Wei & Qin, 2016; Lodise et al. 2022). These frequent storm events induce short but strong wind stress over the surface ocean which triggers several high-frequency (hourly to 10 days) responses at the air-sea and ocean-mixed layer interfaces, which have been shown to impact the air-sea CO_2 flux (FCO_2) significantly (Monteiro et al. 2015, Nicholson et al. 2022). However, despite the persistence of strong storms across the SO, few studies have investigated and quantified the role of storms on the FCO_2 in the SAZ, particularly under different seasonal settings.

FCO_2 is governed by a bulk formulation which constitutes of the gas transfer velocity (k_w) (Ho et al. 2006; Wanninkhof, 2014), the solubility constant (k_o) (Weiss, 1974) and the gradient between the partial pressure of CO_2 in the ocean (pCO_{2sea}) and in the atmosphere (pCO_{2air})

($\Delta pCO_2 = pCO_{2sea} - pCO_{2air}$). The passage of a storm is likely to trigger responses to each of these bulk terms, which may occur in-phase (response time is the same) or out-of-phase (response time is different) with one another. During a storm, strong wind stress will result in stronger k_w (quadratic function of wind speed; Wanninkhof et al. 2014), increasing the magnitude of FCO_2. Importantly, the increase in wind stress may also generate upper ocean dissipation (through shear production and buoyancy loss) which elicits physical transport within and across the mixed layer and its boundaries. This is via vertical (entrainment) and lateral (advection) exchanges of water masses into and out of the mixed layer, increasing or decreasing pCO_{2sea} and ΔpCO_2 (Ito et al. 2016; Nicholson et al. 2022). A 'buoyancy-dominated' phase typically follows this 'momentum-dominated' phase of the storm. The quiescence period post-storm results in a loss in momentum through the drop in wind stress and a gain in buoyancy due to restratification. This can decrease k_o and increase pCO_{2sea} as the solubility of CO_2 decreases (Sarmiento & Gruber, 2006). Above all, it may allow for an increase in the net primary productivity resulting in a net decrease in pCO_{2sea} post-storm during summer (Swart et al. 2015; Nicholson et al. 2016, Carranza et al. 2018; Nicholson et al. 2019; Uchida et al. 2020).

Evidence of storm-driven responses to bulk flux terms has been documented in the subpolar SO, a region of annual mean FCO_2 outgassing (Nicholson et al. 2022). There, strong storm-induced wind stress was linked to increases in FCO_2 through the k_w parameter but also because of concurrent upper ocean mixed layer entrainment of carbon-rich waters, rapidly modifying (reversing and changing the magnitude) the ΔpCO_2, to result in strong outgassing events (Nicholson et al., 2022). Whether storms drive similar responses to both k_w and ΔpCO_2, as well as the phasing of the response of these bulk flux terms, and how it impacts the FCO_2 in the SAZ is yet unclear. However, some insights have been provided by Monteiro et al. (2015) through a conceptual figure, which linked storms to intra-seasonal variations of FCO_2, hypothesizing that storms in the SAZ triggered pCO_{2sea} to increase through entrainment, decreasing the magnitude of ΔpCO_2, causing the FCO_2 ingassing to slightly weaken despite the strong wind stress induced by the storm.

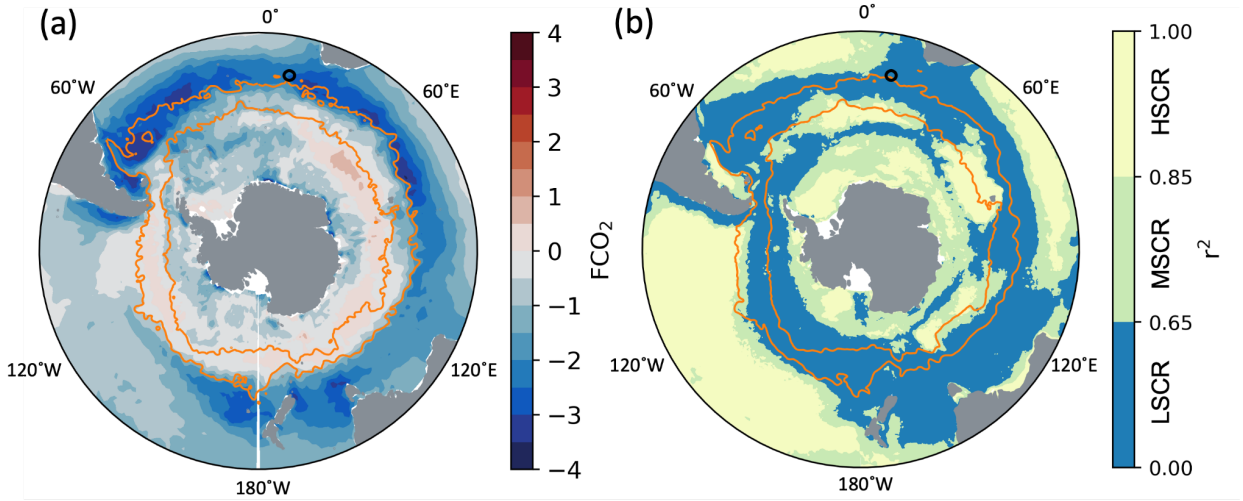

Figure 1: (a) The air-sea CO_2 flux (FCO_2), averaged from monthly CSIR-ML6 data (Gregor et al. 2019) from August 2015 to February 2016, the study period. Negative FCO_2 (in shades of blue) indicates the ingassing of CO_2 and positive FCO_2 (in shades of red) represents the outgassing of CO_2. (b) The spatial characteristics of the seasonal cycle reproducibility (SCR) (method adapted from Thomalla et al. 2011) of pCO_{2sea} obtained from 10 years (2000 to 2009) of NEMO-PISCES simulations, highlighting the low SCR (r^2 = 0 to 0.65; LSCR) of pCO_{2sea} in the majority of the Sub-Antarctic Zone (SAZ). The black circle represents the location where the SOSCEX-III experiment was conducted and the orange contours represent the northern and southern extent of the SAZ from the sea surface height-based definition of the sub-Antarctic Front and the Polar Front (Sokolov & Rintoul, 2009).

Due to the regularity of these storms, such intra-seasonal variability is thought to dominate the seasonality of pCO_{2sea}, a dominant driver of FCO_2 variability, across large regions of the SO (Figure 1b; Monteiro et al. 2015; Gregor et al. 2019; Djeutchouang et al. 2022, Nicholson et al. 2022). However, because of the lack of high-frequency (< 10 days) observations throughout the SO, the mechanisms behind the intra-seasonal variability of FCO_2, that link the storm-driven variability in wind stress directly to the FCO_2 are still not well understood. There remains some debate on what scales of variability are key to accurately estimate the annual mean FCO_2. It has been argued that observed high-frequency variability in k_w only (available using high-resolution reanalysis wind products) is sufficient to capture the intra-seasonal responses of FCO_2 and the corresponding synoptic variability of pCO_{2sea} is of secondary importance to the overall FCO_2 estimates (Bushinsky et al. 2019). Observational evidence from other studies has shown that the phasing of both k_w and pCO_{2sea} to a storm event is important (Monteiro et al. 2015; Nicholson et al. 2022). This suggests that a 10-day or more sampling period may not necessarily capture storm-linked responses on the annual FCO_2 estimates and a sampling resolution of less than 3 days may

be more appropriate to capture such responses in 27.5% of the SO (Djeutchouang et al. 2022) to reduce the annual FCO_2 mean uncertainty to less than 10% (Monteiro et al. 2015).

In this study, we investigate the intra-seasonal changes in FCO_2 associated with storms and hypothesize that the wind-driven constraints on the FCO_2 through rapid modifications of pCO_{2sea} may be as decisive as the high-frequency responses in the k_w parameter. Using high-resolution hourly glider observations, we first provide an explanation of the mechanisms that drive the pCO_{2sea} variability during storms in the SAZ and then proceed to show the importance of considering the temporal aliasing of the pCO_{2sea} and k_w to the strong winds on the FCO_2.

2. Materials and Methods

2.1 Data collection

This study utilized data collected during the third Southern Ocean Seasonal Cycle Experiment (SOSCEx-III) in the SAZ (Further description in text S1 and refer to Swart et al. 2012). This experiment involved the simultaneous deployment of two Liquid Robotics Wave Gliders (WG) (CSIR1 and CSIR2) and two buoyancy profiling Seagliders (SG542 and SG543), which sampled roughly at 8.5°E and 43°S to simulate a pseudo-mooring pattern (Figure S1a).

The WGs sampled from 14th August to 17th October 2015 (CSIR1) and from 9th December 2015 to 8th February 2016 (CSIR2), covering the late winter to the end of the summer period. A modified $MAPCO_2$ sensor made both atmospheric (xCO_{2air}) and oceanic (xCO_{2sea}) observations at hourly temporal resolution with a precision of less than 2 μatm (Sutton et al. 2014). An Airmar XW-200 Ultrasonic Weather station recorded meteorological parameters at 10-minute intervals (further details in Schmidt et al. 2017). The weather station on CSIR1 WG was however faulty, and hourly ERA5 reanalysis wind speed data was used instead (Text S2 elaborates on the choice of reanalysis product).

The Seagliders conducted a total of 1832 profiles over 196 days, measuring the conductivity, temperature, and pressure, amongst others (see Thomalla et al. (2017) for more details), of the first 1000m of the ocean in a V-shaped pattern at a dive cycle of approximately 5

hours. These two deployments resulted in a continuous sampling from 28 July to 8 December 2015 (SG543) and 8 December 2015 to 8 February 2016 (SG542).

2.2 Estimation of the bulk CO_2 flux

The exchange of CO_2 (FCO_2) between the surface ocean and atmosphere can be estimated using a bulk flux formula.

$$FCO_2 = k_w\, k_o\, (pCO_{2sea} - pCO_{2air}) \quad (1)$$

where k_w ($cmhr^{-1}$) is the wind-driven gas transfer velocity (Wanninkhof, 2014), k_o ($molL^{-1}atm^{-1}$) is the solubility of CO_2 in seawater (Weiss, 1974), pCO_{2sea} and pCO_{2air} represent the partial pressure of CO_2 in the ocean and the atmosphere respectively. $pCO_{2sea} - pCO_{2air}$ is commonly represented as ΔpCO_2. Text S2 and S3 describe the quality control and method of calculations of each parameter of the bulk formula.

2.3 Thermal and non-thermal decomposition of pCO_{2sea}

pCO_{2sea} was decomposed into its thermal ($pCO_{2\text{-}th}$; µatm) and non-thermal ($pCO_{2\text{-}nt}$; µatm) components (Takahashi et al. 1993, 2002). $pCO_{2\text{-}th}$ accounts for the thermodynamically dependent characteristics of CO_2 which are driven by the variability in sea surface temperature (SST) while $pCO_{2\text{-}nt}$ accounts for the biophysical processes (vertical mixing and biological consumption) which change the concentration of Dissolved Inorganic Carbon (DIC) in seawater (Takahashi et al., 1993).

$$pCO_{2-th} = pCO_{2sea-mean} \times e^{(0.0423(SST - SST_{mean})} \quad (2)$$

$$pCO_{2-nt} = pCO_{2sea} \times e^{(0.0423(SST_{mean} - SST)} \quad (3)$$

where $pCO_{2sea\text{-}mean}$ and SST_{mean} are the mean of pCO_{2sea} and SST values throughout the entire study period respectively.

3. Results and Discussion

3.1 Observed pCO_{2sea} variability in response to storms.

Here we examine qualitatively how the synoptic-scale momentum-buoyancy dynamics influence the phasing of pCO_{2sea} responses to storms in the SAZ over a significant part of a seasonal cycle. To highlight the atmospheric forcing and upper ocean responses linked to storms, wind stress (a proxy for momentum fluxes), upper ocean stratification (N^2) (a proxy for buoyancy fluxes), and the mixed layer depth (MLD) (momentum-buoyancy balance) were examined (Figures 2a and b). The pCO_{2sea} was also decomposed into its thermal ($pCO_{2\text{-}th}$) and non-thermal component ($pCO_{2\text{-}nt}$) to differentiate biophysical responses ($pCO_{2\text{-}nt}$) from changes in SST ($pCO_{2\text{-}th}$) (Figure 2c).

The study period was characterized by three seasonal regimes (winter, spring, and summer) that represented three different responses of pCO_{2sea} to storms (Figure 2c). During winter, $pCO_{2\text{-}th}$ and $pCO_{2\text{-}nt}$ showed considerable high-frequency response modes (between 1 to 6 hours), at time scales shorter than the wind stress variability (Figures 2a and c). Such high-frequency modes of variability (±5-10 µatm in both $pCO_{2\text{-}th}$ and $pCO_{2\text{-}nt}$) can be indicative of the presence of both sub-mesoscale features (*O*; 1-10 km) (Mahadevan et al. 2004; Lévy et al. 2012) and near-inertial motions (Alford et al. 2016) in the region. Sharp density gradients associated with sub-mesoscale features are short-lived (a few hours to days) and can induce strong vertical advection and mixing (Thomas et al. 2008), which can drive synoptic scale variations in the $pCO_{2\text{-}nt}$ as seen in Figure 2. Similarly, near-inertial waves energised by storms trigger surface vertical mixing on timescale close to the inertial period (17.5 hours at 43.5°S), also driving synoptic changes in the $pCO_{2\text{-}nt}$ (e.g., during W5 and W6, Song et al. 2019, Nicholson et al. 2022).

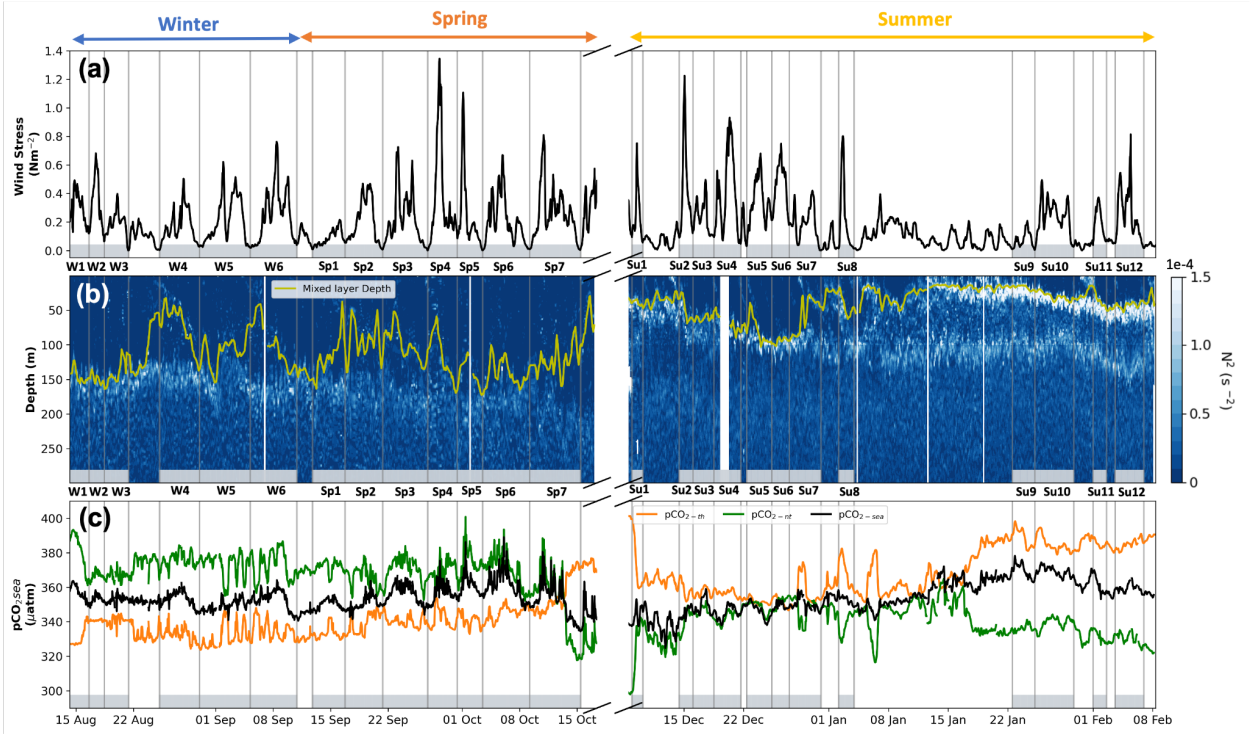

Figure 2: (a) Time series of ERA5 Wind Stress (Nm^{-2}) collocated to the gliders' location at 8.5°E and 43°S. (b) Seaglider observed upper ocean stratification, Brunt Väisälä frequency (N^2; s^{-2}), and mixed layer depth (m; in yellow). Methods for N^2 and MLD calculation can be found in text S3 in the Supplementary Information (c) Wave Glider observed pCO_{2sea} (µatm; in black) and its thermal ($pCO_{2\text{-}th}$ (µatm); in orange) and non-thermal ($pCO_{2\text{-}nt}$ (µatm); in green). The seasonal regimes were defined as a negative net heat flux for winter, an increasing net heat flux for spring, and a stable positive net heat flux for summer (du Plessis et al. 2019). The grey shading highlights the duration of each storm event with storms labelled underneath (Winter: W1-W6, Spring: Sp1-Sp7, and Summer: Su1-Su12), and the grey vertical lines separate each storm (storm identification method can be found in text S4 in the Supplementary Information).

These rapid changes of DIC within the MLD are usually accompanied by rapid temperature changes (Figure 2c). The transport of subsurface water to the surface lowers the temperature within the mixed layer which can decrease the $pCO_{2\text{-}th}$ (by increasing the solubility of CO_2, Sarmiento & Gruber, 2006), hence offsetting the effect of the transported DIC on the overall pCO_{2sea} (Mahadevan et al. 2004, Resplandy et al. 2009). Indeed, for most of winter, these high-frequency modes of variability have little impact on the pCO_{2sea} variability (Figure 2c), likely due to the $pCO_{2\text{-}th}$ and $pCO_{2\text{-}nt}$ terms cancelling each other out (Figure 2c). Instead, the net changes in pCO_{2sea} appear in phase with the wind stress variability linked to storms (Figures 2a and c). During W1 to W6, the pCO_{2sea} showed a small increase and consequent decrease (±5-15 µatm) with the synoptic wind stress cycle. A possible explanation is that the increasing wind stress generated deep mixing,

deepening the MLD (up to ~50 m day^{-1}; Figure 2b) and possibly entraining DIC into the surface mixed layer (as observed in Ko et al. 2021 and Nicholson et al. 2022). As the wind stress decreases post-storm, the mixed layer re-stratifies and shoals the MLD (e.g., between W3 and W4, Figure 2b) until the next storm and the cycle repeats itself. During spring or summer, this quiescent period between storms would typically lead to phytoplankton blooms (Monteiro et al. 2015; Carranza et al. 2018), causing a drop in pCO_{2sea} but the nearly abiotic conditions (<400 mg C m^{-2} d^{-1}, Figure S3) of the SAZ in winter allowed us to eliminate Net Primary Productivity (NPP) as a driver of the pCO_{2sea} changes observed. In addition to entrainment, wind-driven lateral advection of pCO_{2sea} could also drive the synoptic-scale responses in pCO_{2sea} (Figure 2b; Takahashi et al. 2009; Monteiro et al. 2015; Nicholson et al. 2022).

During spring, the intra-seasonal modes of variability in $pCO_{2\text{-}nt}$ (±50 µatm) were much larger than those in $pCO_{2\text{-}th}$ (±15 µatm, Figure 2c). These stronger variations in $pCO_{2\text{-}nt}$ were in turn reflected in the pCO_{2sea} (up to ±55 µatm, comparable to the seasonal variation in pCO_{2sea}) which also varied in phase with the storm wind stress cycle (r^2 = 0.45, Figure 2a). These stronger bursts in pCO_{2sea} could be linked to more intense entrainment events occurring because of stronger storms (>0.75 Nm^{-2}; Figure 2a), and weaker stratification (<0.5x10^{-4} s^{-2}, Figure 2b) in spring compared to winter (0.75 Nm^{-2} and 0.5 – 1.0x10^{-4} s^{-2}). These conditions favour stronger vertical mixing, entraining DIC into the mixed layer (Song et al. 2019; Nicholson et al. 2022). In addition to stronger storm-induced vertical mixing on $pCO_{2\text{-}nt}$, the surface net heat flux gradually increased towards the end of spring (du Plessis et al. 2019) leading to the $pCO_{2\text{-}th}$ to also slowly increase because of warmer SST reducing the solubility of CO_2 (Mahadevan et al. 2004). The contribution of this gradual increase in $pCO_{2\text{-}th}$ and the storm-induced variation on $pCO_{2\text{-}nt}$ led to the observation of the strongest pCO_{2sea} response during Sp6 (±55 µatm) (Figure 2c).

As the surface net heat flux increased further towards the end of spring (du Plessis et al. 2019), the MLD shoaled up to 50 m (Figure 2b). $pCO_{2\text{-}th}$ was observed to exceed the $pCO_{2\text{-}nt}$ on 13 October 2015 (Figure 2c), because of an increase in SST that caused the gradual increase in $pCO_{2\text{-}th}$ and an increased consumption of DIC through NPP that led to the simultaneous gradual

242 decrease in $pCO_{2\text{-nt}}$. This reversal in the $pCO_{2\text{-th}}$ and $pCO_{2\text{-nt}}$ marked the transition from spring to
243 summer regimes in the pCO_{2sea} variability 44 days before the seasonal mixed layer restratification
244 took place (on 26 November 2015 in du Plessis et al. 2019). This highlights the seasonal transition
245 in the primary drivers of pCO_{2sea} variability from a momentum-dominated winter to a combination
246 of momentum and gradually increasing buoyancy-dominated spring ($pCO_{2\text{-th}}$, $r^2 = 0.02$) to finally
247 a thermally and NPP-driven summer ($pCO_{2\text{-th}}$, $r^2 = 0.39$) (Figure 2c).
248
249 As expected, due to the increased solar radiation in summer, the pycnocline stratification
250 strengthened ($0.5x10^{-4}$ – $1.0x10^{-4}$ s^{-2}) and shoaled (50–100 m) during early summer and intensified
251 ($3.0x10^{-4}$ – $4.4x10^{-4}$ s^{-2}) and shoaled (≤50 m) further towards the end of summer (Figure 2b). As
252 the late summer pycnocline layer shoaled and strengthened, the remnant of the winter pycnocline
253 remained below it at approximately 100-150 m (du Plessis et al. 2019), disconnecting the deeper
254 subsurface reservoir of higher DIC from the surface mixed layer (Sprintall et al. 1992; Swart et al.
255 2015). This could explain the reduced sensitivity of pCO_{2sea} to wind stress variations observed
256 across summer (Figures 2a and c). The seasonal warming was also reflected in the slow rise in
257 $pCO_{2\text{-th}}$ (Mahadevan et al. 2004), with variations in $pCO_{2\text{-nt}}$ observed during quiescent periods (e.g.,
258 between Su1 to Su2) because of consumption of DIC by high net primary productivity (Monteiro
259 et al. 2015; Swart et al. 2015; Carranza et al. 2018; Nicholson et al. 2019; Figures 2c and S3).
260
261 **3.2 The influence of the wind on both k_w and ΔpCO_2**
262 Given that pCO_{2sea} responds so sensitively to storm-linked momentum fluxes during
263 winter and spring, does it also influence the synoptic cycle of the CO_2 flux (FCO_2) relative to the
264 wind stress? To examine this question, we focused on three consecutive storms (Sp4, Sp5, and
265 Sp6), which occurred in spring (Figure 3).

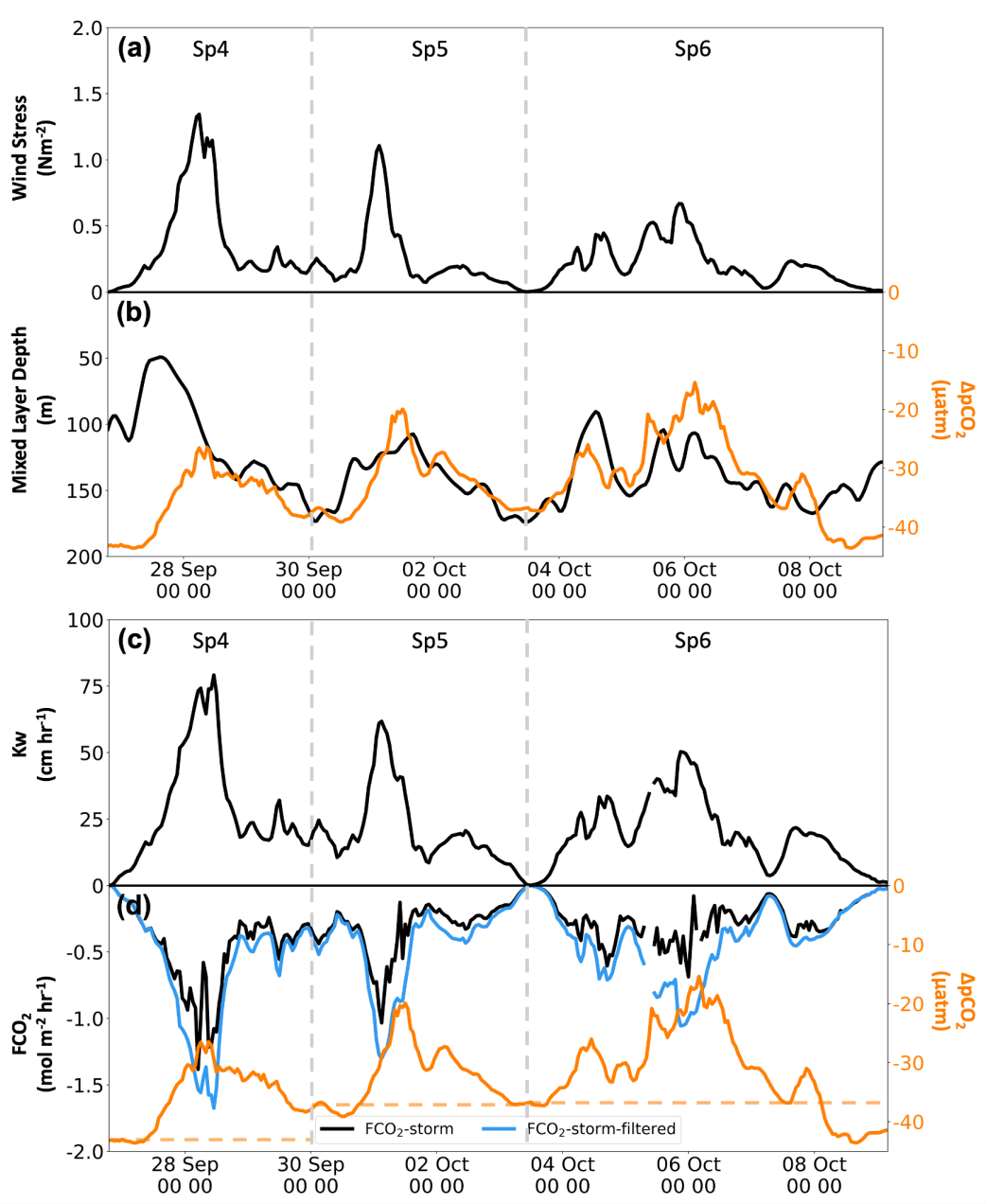

Figure 3: Time series of (a) ERA5 Wind Stress (Nm^{-2}), (b) Mixed Layer Depth (m; in black) and ΔpCO_2 (µatm; in orange), (c) k_w (cm hr^{-1}) and (d) CO_2 flux, FCO_2 (mol m^{-2} hr^{-1}) as observed by the Wave Glider (FCO_{2_storm}; in black) and the storm-filtered FCO_2 ($FCO_{2\_storm\text{-}filtered}$ in blue) calculated from hourly k_w and pre-storm ΔpCO_2 (dashed orange line), for the duration of 3 spring storms events Sp4, Sp5 and Sp6 (27 September 2015 to 9 October 2015).

The variability in ΔpCO_2 is controlled by the air-sea gradient of pCO_{2sea} with negative values implying the ingassing of CO_2. Across the SO, the contribution made by pCO_{2air} variability to ΔpCO_2 is relatively low (1-4 µatm, Tozawa et al. 2021), compared to the seasonal to intra-

seasonal variability in pCO_{2sea} (10-100 µatm, Mongwe et al. 2016, Gregor et al. 2018). Furthermore, while storm linked atmospheric pressure can modulate the pCO_{2air} significantly, it also influences pCO_{2sea} (Text S2), resulting in the net impact of the atmospheric pressure on ΔpCO_2 to be insignificant. Therefore, pCO_{2sea}, and its drivers, have a decisive influence on ΔpCO_2 across the SO (Takahashi et al., 2009, Mongwe et al., 2016), and during the study period ($r^2 = 1$, Figures 2c and 3b). In response to an increase in wind stress, ΔpCO_2 weakened in magnitude (e.g. from -35 to -20 µatm during Sp5) almost in phase with the wind stress with a short lag between each peak varying between 1 to 3 hours throughout all 3 storm events (Figure 3b; brown line). The response of the MLD was, in contrast, out of phase with the wind stress (Figure 3b) which was as expected and can be explained as the delayed response of the MLD due to inertial motion set by the passing storms (Cisewski et al. 2005) and the low responsiveness of the MLD to the wind stress when compared with the active mixing layer (Whitt et al. 2019; Nicholson et al. 2022).

According to the bulk FCO_2 formula, the influence of the wind on the FCO_2 is accounted for through the nonlinear (quadratic) relationship between k_w and the wind speed (Wanninkhof et al. 2014). To examine our hypothesis about how, instead, the high-frequency variability of ΔpCO_2 and k_w are both necessary to capture the magnitude and phasing of the intra-seasonal mean FCO_2, we compared the observed FCO_2 ($FCO_{2\text{-storm}}$) and a calculated FCO_2 which removes the mixing/entrainment response of pCO_{2sea} ($FCO_{2\text{-storm-filtered}}$). The $FCO_{2\text{-storm-filtered}}$ was re-calculated using hourly k_w but with ΔpCO_2 kept constant to its pre-storm value to filter out the storm-driven synoptic response of ΔpCO_2 (Figure 3d – blue line). For this study, using the pre-storm ΔpCO_2 was the best option (Text S4) as it mutes the influence of the previous and following storms on ΔpCO_2 during any storm to have a more accurate estimate of the FCO_2 per storm event.

With each storm, k_w increases in phase with the wind stress (Figure 3c), which, in turn, drove the increase in magnitude of the FCO_2 (Figure 3d, Wanninkhof et al. 2014). The phasing between $FCO_{2\text{-storm}}$ and $FCO_{2\text{-storm-filtered}}$ were similar, i.e., they both varied in phase with each storm because of k_w (Figure 3d). However, because ΔpCO_2 also weakened in response to the increasing wind stress, the magnitude of the $FCO_{2\text{-storm}}$ was lower than the $FCO_{2\text{-storm-filtered}}$. This is also

consistent with the observations in Monteiro et al. (2015) where FCO_2 was observed to weaken despite the increase in wind stress induced by storms. Bushinsky et al. (2019) suggested that the aliasing error from a 10-day sampling frequency of pCO_{2sea} (Monteiro et al. 2015) from biogeochemical profiling floats may not be the primary source of uncertainty in the annual FCO_2 estimate in the SO because hourly wind speed data captures most of the intra-seasonal FCO_2 variability through the k_w term. However, our study shows that, while the k_w term does capture most of the FCO_2 variability, the temporal phasing of the ΔpCO_2 and the k_w throughout a storm event is both needed to not overestimate the intra-seasonal FCO_2 (by up to 0.7 $molm^{-2}hr^{-1}$ during the peak of storm Sp4) because the wind influences both the k_w and the ΔpCO_2 simultaneously (Figure 3d).

3.3 Seasonal-scale implications of storm-induced synoptic variability

The above experiment was replicated for the whole observed time series to further explore the implications of the complex storm-induced impacts on ΔpCO_2 on the integrated seasonal mean FCO_2 (Figure 4). Since both k_w and the wind stress were calculated as a function of the wind speed, they were also strongly correlated ($r^2 = 0.95$; Figures 2a and 4a). The overall contribution of k_o to the synoptic variability of FCO_2 was shown to be very small throughout the study period ($r^2 = 0.06$; Figure 4b). The synoptic scale variability in k_o (up to 0.02 $molm^{-3}atm^{-1}$), was small compared to the magnitude of its seasonal variability (up to 0.1 $molm^{-3}atm^{-1}$), both of which reflected changes in temperature and salinity instead (Figure 4b).

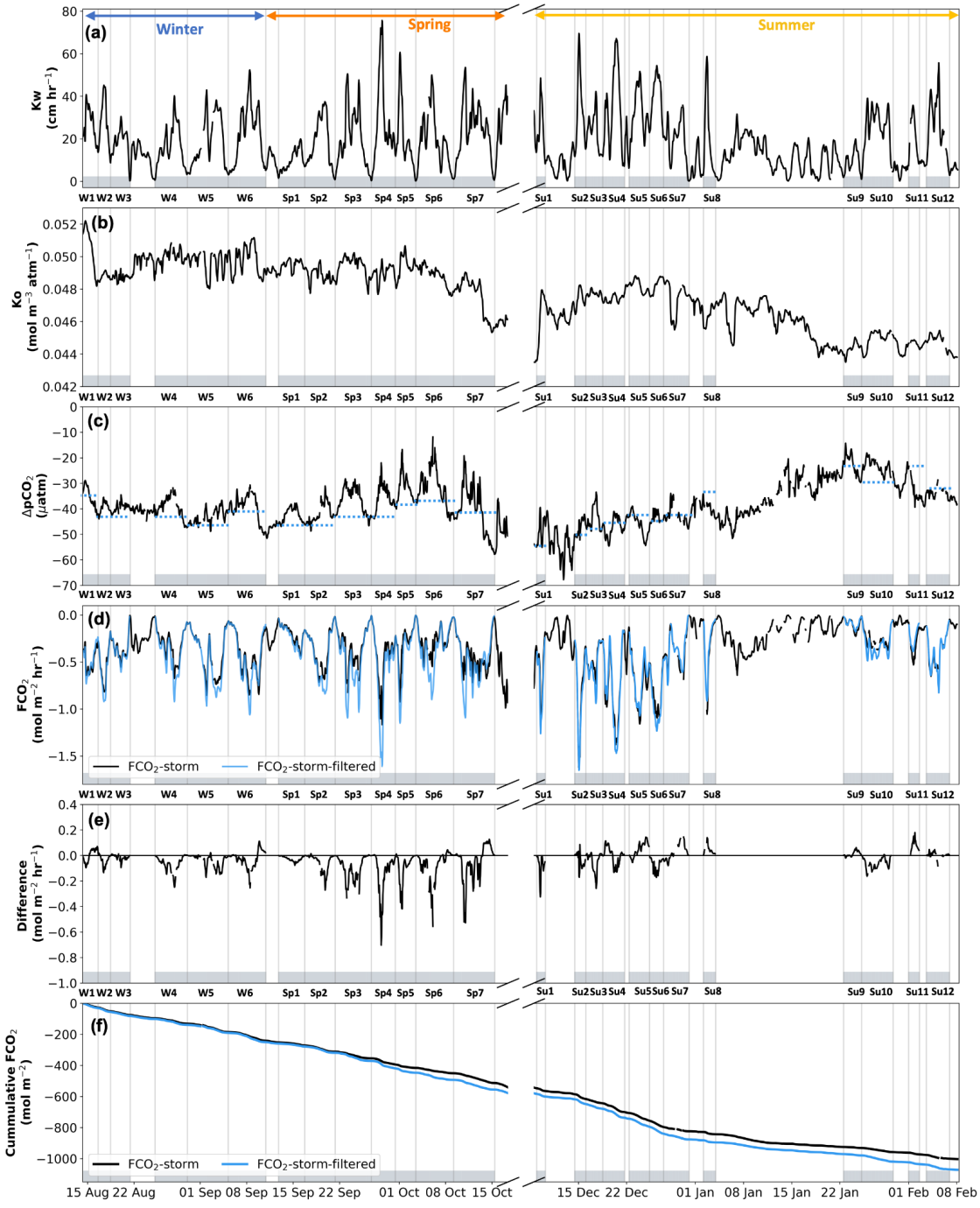

Figure 4: Time series of the **(a)** gas transfer coefficient, k_w (cm hr^{-1}) calculated from ERA5 winds. Wave Glider observations of **(b)** solubility coefficient, k_o (mol L^{-1} atm^{-1}), **(c)** gradient in the partial pressure of CO_2 between the ocean and the atmosphere (ΔpCO_2 (μatm) = pCO_{2sea} (μatm) – pCO_{2air} (μatm)), **(d)** CO_2 flux, FCO_2 (mol m^{-2} hr^{-1}) in black and the storm-filtered FCO_2, with the wind influence through k_w only, in blue, **(e)** difference between the observed FCO_2 and the storm filtered FCO_2 (mol m^{-2} hr^{-1}), **(f)** Cumulative sum of the observed FCO_2 (in black) and storm-filtered FCO_2 (in blue). The grey shading represents the storm occurrences, and the grey lines separate each storm from one another.

Throughout the deployment, ΔpCO_2 was negative indicating a persistent ingassing flux of CO_2, characterized by a strong mode of synoptic-scale variability, at the sampling location (Figure 4c). The magnitude of the re-calculated $FCO_{2\text{-storm-filtered}}$ (excluding the storm-pCO_{2sea} feedback) was consistently stronger than the $FCO_{2\text{-storm}}$ during winter-spring but much less so during summer events (Figure 4d). This is seen through the variability in the magnitude of the difference between the observed and re-calculated fluxes ($FCO_{2\text{-storm}}$ - $FCO_{2\text{-storm-filtered}}$) (Figures 4d and e). It shows that the difference in magnitude was weaker during winter (up to -0.3 $molm^{-2}hr^{-1}$) and strongest during spring (up to -0.7 $molm^{-2}hr^{-1}$) which also coincided with the pronounced synoptic variability in the pCO_{2sea} due to a combination of stronger storms (>0.75 Nm^{-2}), weaker stratification (<0.5x10^{-4} s^{-2}) and the slow seasonal increase of the $pCO_{2\text{-th}}$ component (Figure 2b and c). It also shows that the FCO_2 averaged per storm event can be overestimated by a minimum of 6.6% (W3 and Sp1) to a maximum of 18.3% (W6) in winter and 26.5% (Sp4) in spring if the storm-pCO_{2sea} feedback is omitted from the FCO_2 (Figure 4e).

To examine the integrated impact of storms on the pCO_{2sea}, their cumulative influence on the FCO_2 through most of a seasonal cycle was investigated. The cumulative sum of both the $FCO_{2\text{-storm}}$ (-1003.06 $molm^{-2}$) and $FCO_{2\text{-storm-filtered}}$ (-1069.47 $molm^{-2}$) across winter, spring, and late summer, also showed an overall overestimation bias of 6.41% (Figure 4f), suggesting that not accounting for the storm driven responses in pCO_{2sea} on the FCO_2, over a significant portion of a seasonal cycle, introduces a bias in the annual cumulative FCO_2 uptake. At the study location, each storm had a lifespan of 1.5 to 7 days. Autonomous floats with a 10-day sampling frequency (Johnson et al. 2017) could thus have a limited probability (<10 %, Monteiro et al. 2015) of capturing the entire synoptic cycle of pCO_{2sea} (Figure 2c), resulting in the intra-seasonal FCO_2 variability in the SAZ not being appropriately captured (Figure 4d, Monteiro et al. 2015, Djeutchouang et al. 2022). Our results provide an initial mechanistic analysis, which support the findings of Monteiro et al. (2015) (and thereafter Djeutchouang et al. 2022), showing why a 3-day or less sampling period is necessary to reduce the uncertainties in the annual mean FCO_2 estimates in the SAZ.

This study was conducted in the SAZ, a region characterised by frequent storms and mesoscale features which disrupts the seasonal cycle of pCO_{2sea} leading to this region to be

dominated by intra-seasonal modes of pCO_{2sea} variability (Figure 1b; Monteiro et al. 2015, Gregor et al. 2019, Djeutchouang et al. 2022). From a Seasonal Cycle Reproducibility (SCR) metric (Figure 1b), formulated from a mesoscale resolving model for the SO, we thus propose that the findings of this study will project to the low SCR regions, which extends to 25 to 30% of the SO (Figure 1b), and emphasize the need for high frequency (< 3 days) pCO_{2sea} observations in such regions.

4. Synthesis

This study hypothesized that the influence of high-frequency wind variability induced by storms on pCO_{2sea} contributes significantly to mean estimates of FCO_2 on seasonal to annual time scales. We showed that the wind simultaneously influences two terms of the FCO_2 bulk equation: k_w and ΔpCO_2, and that this influence was seasonally sensitive. Three main conclusions could be framed from this study.

First, the influence of the storm-driven wind on hourly pCO_{2sea} observations in the SAZ was strongly seasonal. Across winter and spring, the mechanistic response of pCO_{2sea} appeared mostly momentum-dominated, i.e., wind-induced entrainment and lateral advection during storm events drove most of its variability (Figure 2), with the influence of NPP being very small to undetectable (Figure S3). During summer, pCO_{2sea} variability seemed predominantly affected by NPP and changes in the SST, with pCO_{2sea} responses to the storm-driven wind variability being weakly sensitive (Figure 2). Future work and experiments will include observations of turbulent mixing to provide a more quantitative analysis of the associated mechanisms to discern the vertical entrainment of DIC from horizontal advection (e.g., Nicholson et al. 2022).

Second, based on these seasonally different mechanistic responses in pCO_{2sea}, storms have been shown to counterintuitively weaken the FCO_2, due to the weakening in the magnitude of ΔpCO_2, despite the increase in k_w, throughout winter and spring (Figure 4). This highlights the

importance of sampling ΔpCO_2 at high frequencies to minimize a potential overestimation of the FCO_2 uptake by up to 18.3% in winter and 26.5% in spring.

Finally, the integrated influence of these synoptic scale overestimations of the FCO_2 over an entire seasonal cycle, showed that the cumulative sum of the strength of FCO_2 uptake could be overestimated by 6.41% (Figure 4e) and this bias can be projected to 25 to 30% of the area of the SO (Figure 1).

Acknowledgments

This work is part of the Ph.D. of Tesha Toolsee who was partially funded by the South African National Research Foundation (NRF grant: MND210514601456/145319) and the Council of Scientific and Industrial Research (CSIR) Doctoral Studentship funds. PMS Monteiro and S.-A Nicholson are supported by the European Union's Horizon 2020 research and innovation program under Grant 821001 (SO-CHIC) and the NRF-SANAP (SNA170522231782, SANAP200324510487). The authors of this work would like to thank SANAP and the captain and crew of the S. A. Agulhas II, as well as Sea Technology Services for their contribution in the deployment and retrieval of the gliders.

Open Research

The Wave Glider and Profiling buoyancy glider data were provided by the Southern Ocean Carbon and Climate Observatory (SOCCO-CSIR). ERA5 reanalysis wind speeds, wind stress, and pressure data were produced by the European Centre for Medium-Range Weather Forecasts (ECMWF), and obtained from https: //cds.climate.copernicus.eu/cdsapp#!/dataset/reanalysis-era5-pressurelevels?tab=overview and accessed on 1 March 2022. CSIR-ML6 data version 2019a is available from Ocean Carbon Data system (OCADS; https://doi.org/10.25921/z682-mn47, Gregor et al., 2019).

References

Alford, M. H., MacKinnon, J. A., Simmons, H. L., & Nash, J. D. (2016). Near-inertial internal gravity waves in the ocean. Annual Review of Marine Science, 8, 95–123. https://doi.org/10.1146/annurev-marine-010814-015746

Bates, N.R., Knap, A.H., and Michaels, A.F. (1998). Contribution of hurricanes to local and global estimates of air–sea exchange of CO_2. Nature, 395(6697), 58-61, https://doi.org/10.1038/25703.

Bronselaer, B., Zanna, L., Munday, D. R., & Lowe, J. (2018). Southern Ocean carbon-wind stress feedback. Climate Dynamics, 51, 2743–2757, https://doi.org/10.1007/s00382-017-4041-y.

Bushinsky, S.M., Landschützer, P., Rödenbeck, C., Gray, A.R., Baker, D., Mazloff, M.R., Resplandy, L., Johnson, K.S. and Sarmiento, J.L. (2019). Reassessing Southern Ocean air-sea CO_2 flux estimates with the addition of biogeochemical float observations. Global Biogeochemical Cycles, 33(11), 1370–1388, https://doi.org/10.1029/2019GB006176.

Caldeira, K., & Duffy, P. B. (2000). The role of the Southern Ocean in uptake and storage of anthropogenic carbon dioxide. Science, 287(5453), 620–622, https://doi.org/10.1126/science.287.5453.620.

Carranza, M. M., & Gille, S. T. (2015). Southern Ocean wind-driven entrainment enhances satellite chlorophyll-a through the summer. Journal of Geophysical Research: Oceans, 120(1), 304–323, https://doi.org/10.1002/2014JC010203.

Carranza, M. M., Gille, S. T., Franks, P. J., Johnson, K. S., Pinkel, R., & Girton, J. B. (2018). When mixed layers are not mixed. storm-driven mixing and bio-optical vertical gradients in mixed layers of the Southern Ocean. Journal of Geophysical Research: Oceans, 123(10), 7264–7289, https://doi.org/10.1029/2018JC014416.

Cisewski, B., Strass, V. H., & Prandke, H. (2005). Upper-ocean vertical mixing in the Antarctic polar front zone. Deep Sea Research Part II: Topical Studies in Oceanography, 52(9-10), 1087–1108, https://doi.org/10.1016/j.dsr2.2005.01.010.

DeVries, T., Holzer, M., & Primeau, F. (2017). Recent increase in oceanic carbon uptake driven by weaker upper-ocean overturning. Nature, 542(7640), 215–218, https://doi.org/10.1038/nature21068.

Djeutchouang, L. M., Chang, N., Gregor, L., Vichi, M., & Monteiro, P. (2022). The sensitivity of pCO_2 reconstructions to sampling scales across a Southern Ocean sub-domain: a semi-idealized ocean sampling simulation approach. Biogeosciences, 19(17), 4171–4195, https://doi.org/10.5194/bg-19-4171-2022.

Du Plessis, M., Swart, S., Ansorge, I. J., Mahadevan, A., & Thompson, A. F. (2019). Southern Ocean seasonal restratification delayed by submesoscale wind–front interactions. Journal of Physical Oceanography, 49(4), 1035–1053, https://doi.org/10.1175/JPO-D-18-0136.1.

Emerson, S., & Hedges, J. (2008). Chemical oceanography and the marine carbon cycle. Cambridge University Press, ISBN: 978-1-139-47161-9.

Gloege, L., McKinley, G.A., Landschützer, P., Fay, A.R., Frölicher, T.L., Fyfe, J.C., Ilyina, T., Jones, S., Lovenduski, N.S., Rodgers, K.B. and Schlunegger, S., (2021). Quantifying errors in observationally based estimates of ocean carbon sink variability. Global Biogeochemical Cycles, 35(4), https://doi.org/10.1029/2020GB006788.

Gregor, L., Kok, S. and Monteiro, P.M. (2018). Interannual drivers of the seasonal cycle of CO 2 in the Southern Ocean. Biogeosciences, 15(8), 2361-2378, https://doi.org/10.5194/bg-15-2361-2018.

Gregor, L., Lebehot, A. D., Kok, S., & Scheel Monteiro, P. M. (2019). A comparative assessment of the uncertainties of global surface ocean pCO_2 estimates using a machine-learning

ensemble (CSIR-ML6 version 2019a)–Have we hit the wall? Geoscientific Model Development, 12(12), 5113–5136, https://doi.org/10.5194/gmd-12-5113-2019.

Gruber, N., Clement, D., Carter, B.R., Feely, R.A., Van Heuven, S., Hoppema, M., Ishii, M., Key, R.M., Kozyr, A., Lauvset, S.K. and Lo Monaco, C. (2019). The oceanic sink for anthropogenic CO_2 from 1994 to 2007. Science, 363(6432), 1193–1199, https://doi.org/10.1126/science.aau5153.

Ho, D. T., Law, C. S., Smith, M. J., Schlosser, P., Harvey, M., & Hill, P. (2006). Measurements of air-sea gas exchange at high wind speeds in the Southern Ocean: Implications for global parameterizations. Geophysical Research Letters, 33(16), https://doi.org/10.1029/2006GL026817.

Ito, R.G., Garcia, C.A.E. and Tavano, V.M. (2016). Net sea-air CO_2 fluxes and modelled pCO_2 in the southwestern subtropical Atlantic continental shelf during spring 2010 and summer 2011. Continental Shelf Research, 119, 68-84, https://doi.org/10.1016/j.csr.2016.03.013.

Ko, Y. H., Park, G.-H., Kim, D., & Kim, T.-W. (2021). Variations in seawater pCO_2 associated with vertical mixing during tropical cyclone season in the north-western subtropical Pacific Ocean. Frontiers in Marine Science, 8, 679314, https://doi.org/10.3389/fmars.2021.679314.

Lévy, M., Lengaigne, M., Bopp, L., Vincent, E.M., Madec, G., Éthé, C., Kumar, D. and Sarma, V.V.S.S., (2012). Contribution of tropical cyclones to the air-sea CO_2 flux: A global view. Global Biogeochemical Cycles, 26(2), https://doi.org/10.1029/2011GB004145.

Lévy, M., Ferrari, R., Franks, P.J., Martin, A.P. and Rivière, P., (2012). Bringing physics to life at the submesoscale. Geophysical Research Letters, *39*(14), https://doi.org/10.1029/2012GL052756.

Li, Z., England, M. H., Groeskamp, S., Cerovečki, I., & Luo, Y. (2021). The origin and fate of subantarctic mode water in the Southern Ocean. Journal of Physical Oceanography, 51(9), 2951–2972, https://doi.org/10.1175/JPO-D-20-0174.1.

Lodise, J., Merrifield, S., Collins, C., Rogowski, P., Behrens, J., & Terrill, E. (2022). Global climatology of extratropical cyclones from a new tracking approach and associated wave heights from satellite radar altimeter. Journal of Geophysical Research: Oceans, 127(11), https://doi.org/10.1029/2022JC018925.

Mahadevan, A., Lévy, M. and Mémery, L., (2004). Mesoscale variability of sea surface pCO_2: What does it respond to? Global Biogeochemical Cycles, 18(1), https://doi.org/10.1029/2003GB002102.

Mongwe, N. P., Chang, N., & Monteiro, P. M. (2016). The seasonal cycle as a mode to diagnose biases in modelled CO_2 fluxes in the Southern Ocean. Ocean Modelling, 106, 90–103, https://doi.org/10.1016/j.ocemod.2016.09.006.

Monteiro, P. M., Gregor, L., Lévy, M., Maenner, S., Sabine, C. L., & Swart, S. (2015). Intraseasonal variability linked to sampling alias in air-sea CO_2 fluxes in the Southern Ocean. Geophysical Research Letters, 42(20), 8507–8514, https://doi.org/10.1002/2015GL066009.

Nicholson, S.-A., Lévy, M., Jouanno, J., Capet, X., Swart, S., & Monteiro, P. M. (2019). Iron supply pathways between the surface and subsurface waters of the Southern Ocean: from winter entrainment to summer storms. Geophysical Research Letters, 46 (24), 14567–14575, https://doi.org/10.1029/2019GL084657.

Nicholson, S.A., Whitt, D.B., Fer, I., du Plessis, M.D., Lebéhot, A.D., Swart, S., Sutton, A.J. and Monteiro, P.M., (2022). Storms drive outgassing of CO_2 in the subpolar Southern Ocean. Nature communications, 13(1), 158, https://doi.org/10.1038/s41467-021-27780-w.

Resplandy, L., Lévy, M., d'Ovidio, F. and Merlivat, L., (2009). Impact of submesoscale variability in estimating the air-sea CO2 exchange: Results from a model study of the POMME experiment. Global Biogeochemical Cycles, 23(1), https://doi.org/10.1029/2008GB003239.

Sabine, C.L., Feely, R.A., Gruber, N., Key, R.M., Lee, K., Bullister, J.L., Wanninkhof, R., Wong, C.S.L., Wallace, D.W., Tilbrook, B. and Millero, F.J. (2004). The oceanic sink for anthropogenic CO_2. Science, 305(5682), 367–371, https://doi.org/10.1126/science.1097403.

Sarmiento, J. & Gruber, N. (2006). Ocean biogeochemical dynamics. Princeton, NJ: Princeton University Press, https://doi.org/10.1515/9781400849079.

Schmidt, K.M., Swart, S., Reason, C. and Nicholson, S.A., (2017). Evaluation of satellite and reanalysis wind products with in-situ wave glider wind observations in the Southern Ocean. Journal of atmospheric and oceanic technology, 34(12), 2551-2568, https://doi.org/10.1175/JTECH-D-17-0079.1.

Sokolov, S.; Rintoul, S. (2009). Circumpolar structure, and distribution of the Antarctic Circumpolar Current fronts: 1. Mean circumpolar paths. Journal of Geophysical Research: Earth Surface, 114, 1–15, https://doi.org/10.1029/2008JC005108.

Song, H., Marshall, J., Campin, J.M. and McGillicuddy Jr, D.J., (2019). Impact of near-inertial waves on vertical mixing and air-sea CO_2 fluxes in the Southern Ocean. Journal of Geophysical Research: Oceans, 124(7), 4605-4617, https://doi.org/10.1029/2018JC014928.

Sprintall, J., & Tomczak, M. (1992). Evidence of the barrier layer in the surface layer of the tropics. Journal of Geophysical Research: Oceans, 97(C5), 7305–7316, https://doi.org/10.1029/92JC00407.

Swart, S., Chang, N., Fauchereau, N., Joubert, W., Lucas, M., Mtshali, T., Roychoudhury, A., Tagliabue, A., Thomalla, S., Waldron, H. and Monteiro, P. (2012). Southern Ocean Seasonal Cycle Experiment 2012: Seasonal scale climate and carbon cycle links. South African Journal of Science, 108(3-4), 11-13, http://dx.doi.org/10.4102/sajs.v108i3/4.1089.

Swart, S., Thomalla, S. J., & Monteiro, P. M. (2015). The seasonal cycle of mixed layer dynamics and phytoplankton biomass in the sub-Antarctic zone: A high-resolution glider experiment. Journal of Marine Systems, 147, 103–115, https://doi.org/10.1016/j.jmarsys.2014.06.002.

Takahashi, T., Olafsson, J., Goddard, J. G., Chipman, D. W., & Sutherland, S. (1993). Seasonal variation of CO_2 and nutrients in the high-latitude surface oceans: A comparative study. Global Biogeochemical Cycles, 7(4), 843–878, https://doi.org/10.1029/93GB02263.

Takahashi, T., Sutherland, S.C., Sweeney, C., Poisson, A., Metzl, N., Tilbrook, B., Bates, N., Wanninkhof, R., Feely, R.A., Sabine, C. and Olafsson, J. (2002). Global sea–air CO_2 flux based on climatological surface ocean pCO_2, and seasonal biological and temperature effects. Deep Sea Research Part II: Topical Studies in Oceanography, 49 (9-10), 1601–1622, https://doi.org/10.1016/S0967-0645(02)00003-6.

Takahashi, T., Sutherland, S.C., Wanninkhof, R., Sweeney, C., Feely, R.A., Chipman, D.W., Hales, B., Friederich, G., Chavez, F., Sabine, C. and Watson, A. (2009). Climatological mean and decadal change in surface ocean pCO_2, and net sea–air CO_2 flux over the global oceans. Deep Sea Research Part II: Topical Studies in Oceanography, 56(8-10), 554–577, https://doi.org/10.1016/j.dsr2.2008.12.009.

Thomalla, S., Fauchereau, N., Swart, S., & Monteiro, P. (2011). Regional scale characteristics of the seasonal cycle of chlorophyll in the Southern Ocean. Biogeosciences, 8(10), 2849–2866, https://doi.org/10.5194/bg-8-2849-2011.

Thomalla, S.J., Moutier, W., Ryan-Keogh, T.J., Gregor, L. and Schütt, J., (2018). An optimized method for correcting fluorescence quenching using optical backscattering on autonomous platforms. Limnology and Oceanography: Methods, 16(2), 132-144, https://doi.org/10.1002/lom3.10234.

561 Thomas, L.N., Tandon, A. and Mahadevan, A. (2008). Submesoscale processes and
562 dynamics. Ocean modelling in an Eddying Regime, 177, 17-38, https://doi.org/10.1029/177GM04.

563 Tozawa, M., Nomura, D., Nakaoka, S.I., Kiuchi, M., Yamazaki, K., Hirano, D., Aoki, S.,
564 Sasaki, H. and Murase, H., (2022). Seasonal variations and drivers of surface ocean pCO_2 in the
565 seasonal ice zone of the eastern Indian sector, Southern Ocean. Journal of Geophysical Research:
566 Oceans, 127(1), https://doi.org/10.1029/2021JC017953.

567 Uchida, T., Balwada, D., P. Abernathey, R., A. McKinley, G., K. Smith, S., & Lévy, M.
568 (2020). Vertical eddy iron fluxes support primary production in the open Southern Ocean. Nature
569 Communications, 11(1), 1125, https://doi.org/10.1038/s41467-020-14955-0.

570 Wanninkhof, R. (1992). Relationship between wind speed and gas exchange over the
571 ocean. Journal of Geophysical Research: Oceans, 97(C5), 7373–7382,
572 https://doi.org/10.1029/92JC00188.

573 Wanninkhof, R. (2014). Relationship between wind speed and gas exchange over the ocean
574 revisited. Limnology and Oceanography: Methods, 12(6), 351–362,
575 https://doi.org/10.4319/lom.2014.12.351.

576 Wei, L., & Qin, T. (2016). Characteristics of cyclone climatology and variability in the
577 Southern Ocean. Acta Oceanologica Sinica, 35, 59–67, https://doi.org/10.1007/s13131-016-0913-
578 y.

579 Weiss, R. (1974). Carbon dioxide in water and seawater: the solubility of a non-ideal gas.
580 Marine Chemistry, 2(3), 203–215, https://doi.org/10.1016/0304-4203(74)90015-2.

581 Whitt, D., Nicholson, S., & Carranza, M. (2019). Global impacts of sub-seasonal (<60
582 days) wind variability on ocean surface stress, buoyancy flux, and mixed layer depth. Journal of
583 Geophysical Research: Oceans, 124(12), 8798–883, https://doi.org/10.1029/2019JC015166.

584 Yuan, X. (2004). High-wind-speed evaluation in the Southern Ocean. Journal of
585 Geophysical Research: Atmospheres, 109(D13), https://doi.org/10.1029/2003JD004179.

Figure 1.

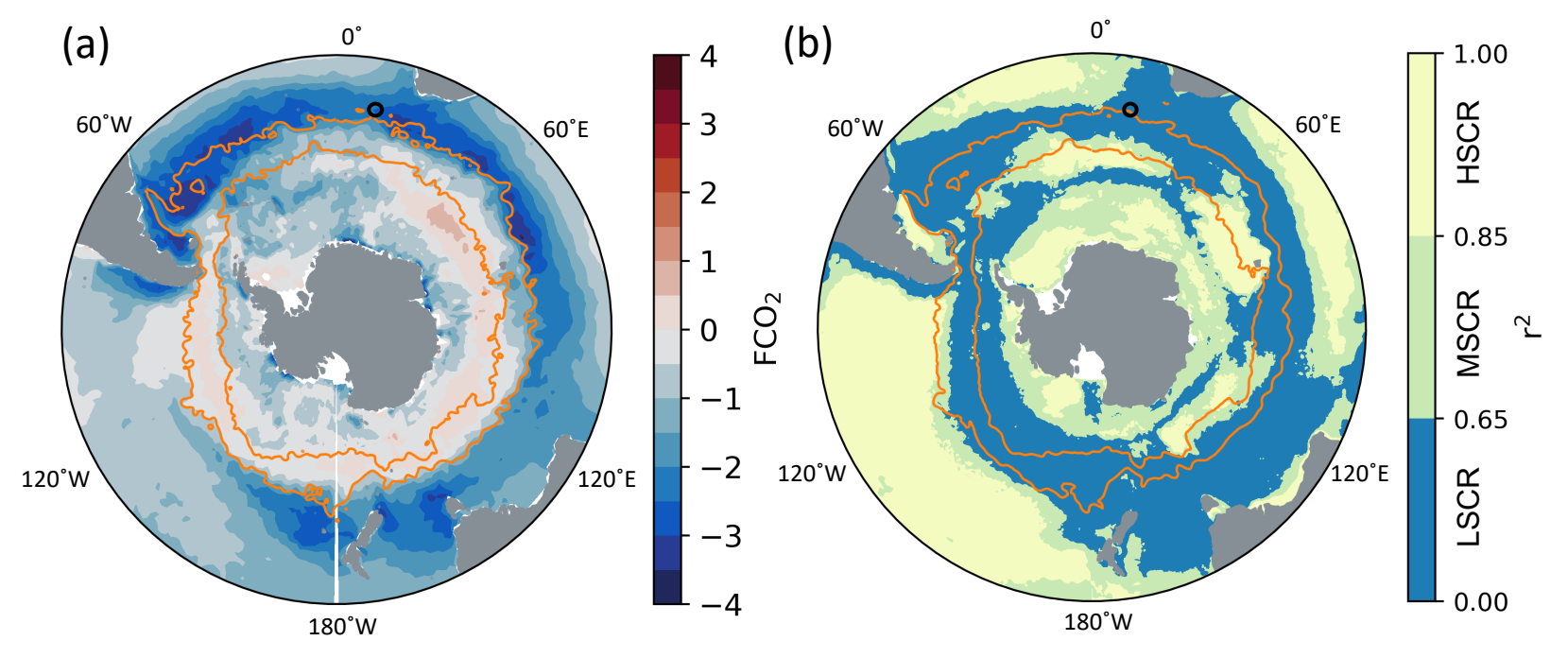
(a)
0˚
60˚W
60˚E
120˚W
120˚E
180˚W
4
3
2
1
0
−1
−2
−3
−4
FCO2
(b)
0˚
60˚W
60˚E
120˚W
120˚E
180˚W
1.00
0.85
0.65
0.00
HSCR
MSCR
LSCR
r2

Figure 2.

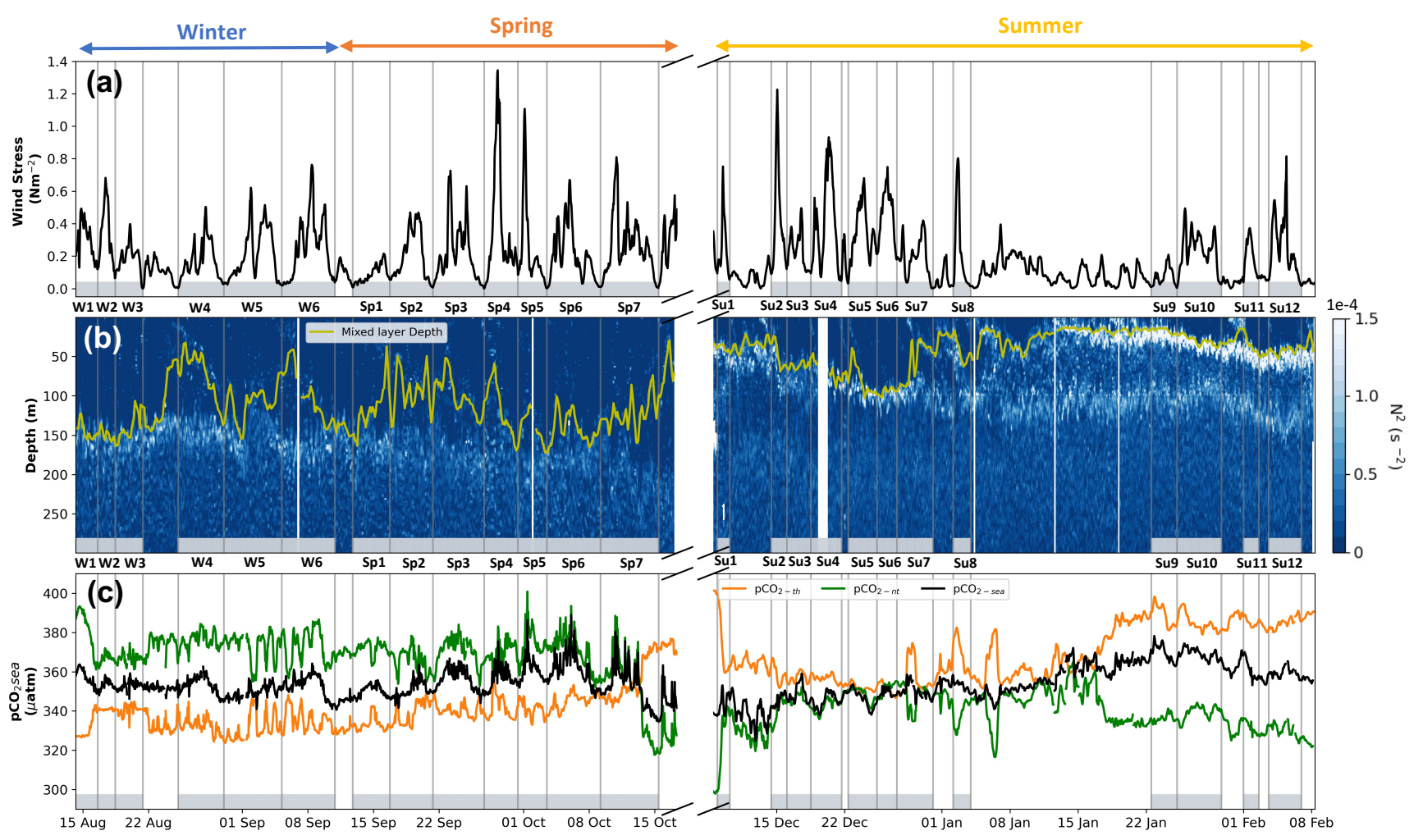
Winter
Spring
Summer
(a)
Wind Stress (Nm^{-2})
1.4
1.2
1.0
0.8
0.6
0.4
0.2
0.0
W1 W2 W3 W4 W5 W6 Sp1 Sp2 Sp3 Sp4 Sp5 Sp6 Sp7
Su1 Su2 Su3 Su4 Su5 Su6 Su7 Su8 Su9 Su10 Su11 Su12
(b)
Mixed layer Depth
Depth (m)
50
100
150
200
250
1e-4
1.5
1.0
0.5
0
N^2 (s^{-2})
(c)
pCO_{2-th}
pCO_{2-nt}
pCO_{2-sea}
pCO_2sea (μatm)
400
380
360
340
320
300
15 Aug
22 Aug
01 Sep
08 Sep
15 Sep
22 Sep
01 Oct
08 Oct
15 Oct
15 Dec
22 Dec
01 Jan
08 Jan
15 Jan
22 Jan
01 Feb
08 Feb

Figure 3.

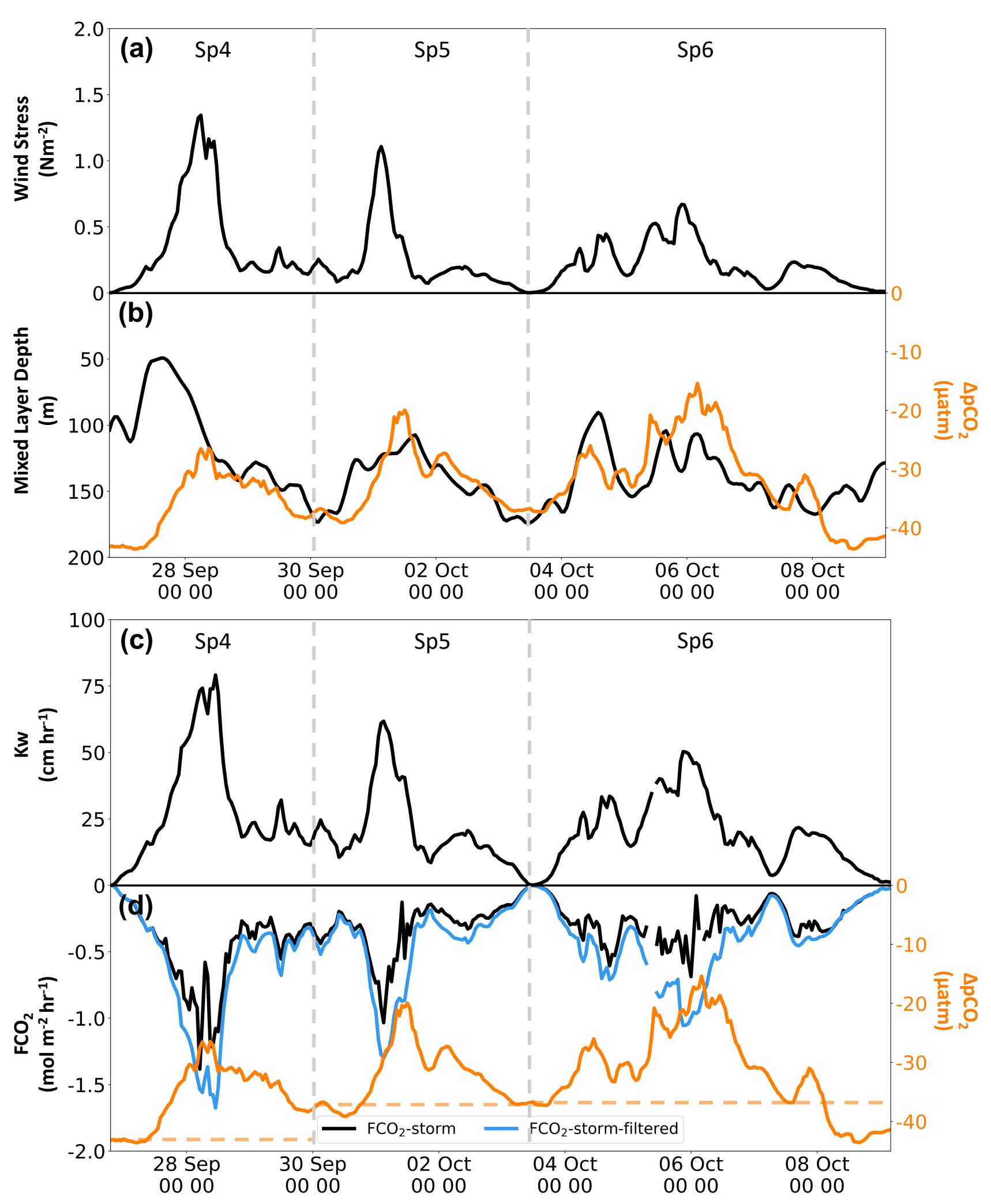
(a)
Sp4
Sp5
Sp6
Wind Stress (Nm-2)
2.0
1.5
1.0
0.5
0
(b)
Mixed Layer Depth (m)
50
100
150
200
-10
-20
-30
-40
ΔpCO2 (μatm)
28 Sep 00 00
30 Sep 00 00
02 Oct 00 00
04 Oct 00 00
06 Oct 00 00
08 Oct 00 00
(c)
Kw (cm hr-1)
100
75
50
25
0
(d)
FCO2 (mol m-2 hr-1)
-0.5
-1.0
-1.5
-2.0
FCO2-storm
FCO2-storm-filtered

Figure 4.

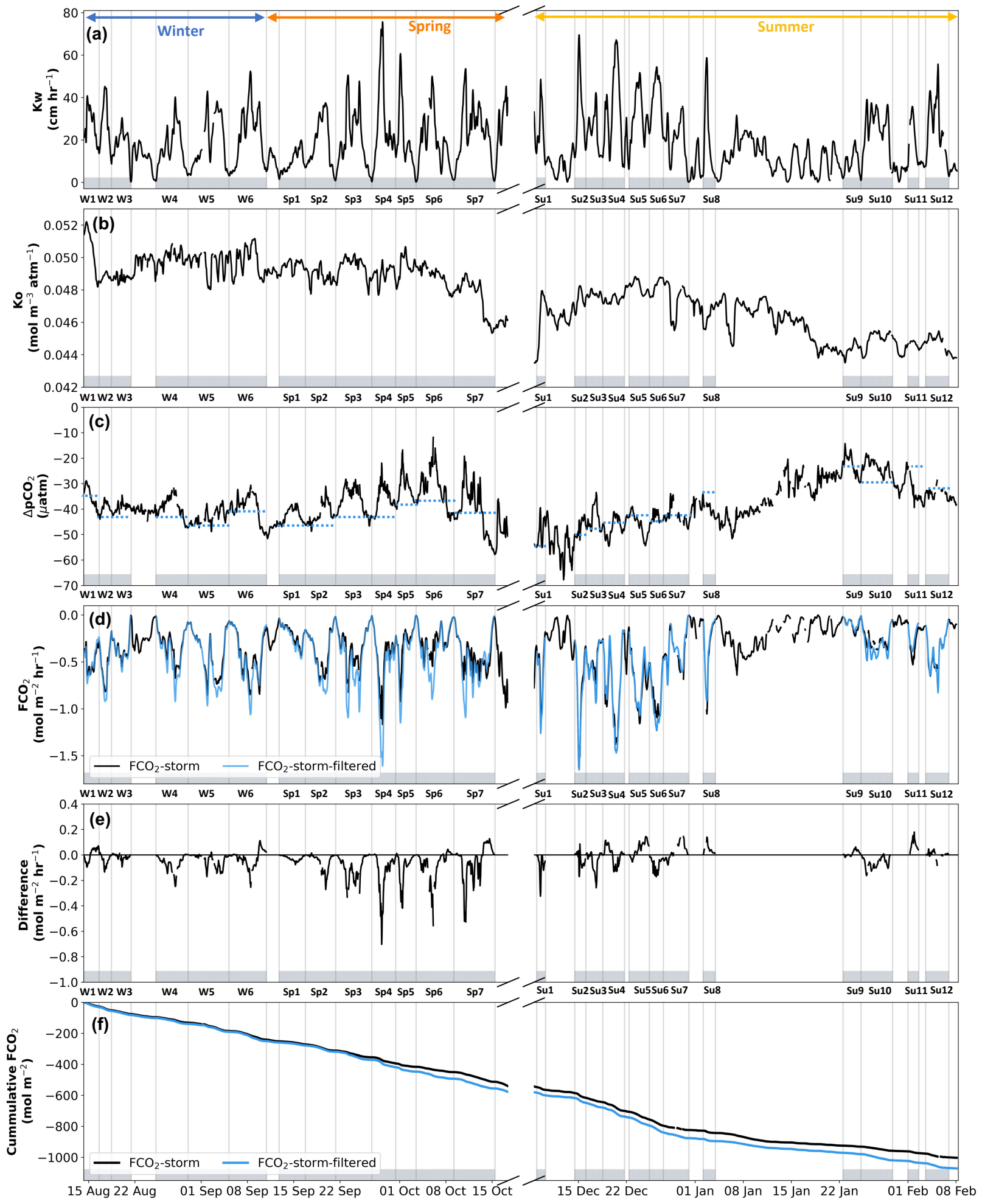
(a)
Winter
Spring
Summer
Kw (cm hr^{-1})
(b)
Ko (mol m^{-3} atm^{-1})
(c)
ΔpCO$_2$ (μatm)
(d)
FCO$_2$ (mol m^{-2} hr^{-1})
FCO$_2$-storm
FCO$_2$-storm-filtered
(e)
Difference (mol m^{-2} hr^{-1})
(f)
Cummulative FCO$_2$ (mol m^{-2})
FCO$_2$-storm
FCO$_2$-storm-filtered
W1 W2 W3 W4 W5 W6 Sp1 Sp2 Sp3 Sp4 Sp5 Sp6 Sp7 Su1 Su2 Su3 Su4 Su5 Su6 Su7 Su8 Su9 Su10 Su11 Su12
15 Aug 22 Aug 01 Sep 08 Sep 15 Sep 22 Sep 01 Oct 08 Oct 15 Oct 15 Dec 22 Dec 01 Jan 08 Jan 15 Jan 22 Jan 01 Feb 08 Feb